Environmental Fluid Mechanics (2025) 25:16
https://doi.org/10.1007/s10652-025-10026-4

ORIGINAL ARTICLE

Three-dimensional modeling of diffusion-gravity flows in ice-covered lakes

Fatemeh Sadat Sharifi[1,2] · Reinhard Hinkelmann[2] · Tore Hattermann[3] · Georgiy Kirillin[1]

Received: 9 August 2024 / Accepted: 18 January 2025

Abstract
When a solid inclined surface is submerged in a quiescent stratified fluid, the combined effects of buoyancy forces and diffusion generate an upward gravity flow along the slope. Thermally stratified ice-covered lakes remain in a nearly quiescent state and are potentially prone to this effect. We use three-dimensional hydrodynamic modeling to investigate the diffusion-gravity flow and its impact on lake-wide circulation in idealized ice-covered lakes. The qualitative characteristics of the boundary flow were adequately simulated by the model, supported by a good agreement with theoretical predictions. In enclosed lakes, the modeled diffusion-driven boundary flow generates residual circulation, which overturns the entire lake water column within 1 to 6 months, suggesting a significant contribution of this mechanism to heat and mass transport in lakes with long ice-covered seasons. When the insulation boundary condition is lifted and additional buoyancy is produced by heat flux from lake sediment, a counterflow emerges, resulting in a circulation pattern characterized by the superposition of two opposing boundary flows. At flux magnitudes exceeding one watt per square meter, the counterflow can entirely replace the diffusion-driven circulation. Due to the small magnitudes of these flows, the Coriolis effect substantially influences circulation, partially transforming radial flow into rotational lake-wide "gyres." The number and rotational direction of these gyres depend on the relative contribution of bottom heat flux. The results provide a framework for designing field studies in real lakes and investigating circulation effects on the transport of dissolved matter, such as nutrients, oxygen and greenhouse gases in ice-covered lakes.

Keywords Diffusion-gravity flow · Thermal stratification · Lake circulation · Lake ice · Sediment heat storage · Bottom boundary layer

1 Introduction

Circulation in ice-covered lakes is distinguished by several features making it a specific problem in environmental fluid dynamics: the absence of wind shear on the lake surface, closed lateral boundaries, fixed temperature at the ice base, and persistent stable density stratification at water temperatures below the maximum density value, T_{md} ([1,

Extended author information available on the last page of the article

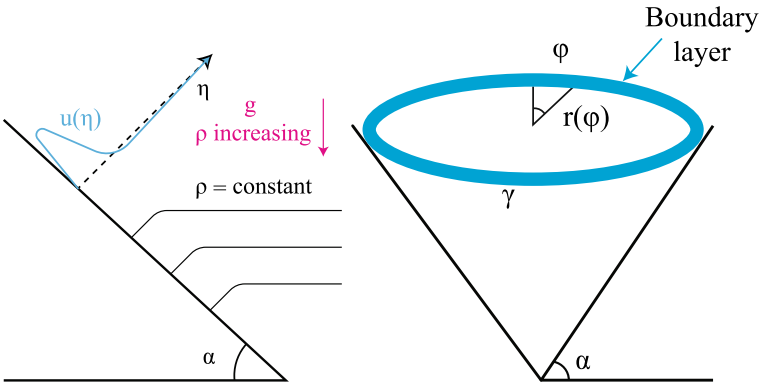

Fig. 1 Schematic of upslope diffusion-driven flow

2]). As a result, the external driving forces of the circulation are limited and the flow is slow compared to that in open waters. The most energetic driver of vertical mixing and horizontal currents is the buoyancy produced by solar radiation penetrating the ice cover [3, 4]. The buoyancy production by solar radiation can be prevented by snow cover [1, 5] and is virtually absent in polar regions during the polar night. The second important driver of buoyancy-driven flows is the release of heat stored in sediment during the open water period, creating horizontal density gradients and thus producing a downward flow driven by density along the bottom slopes [6]. The mechanism is particularly relevant at the earlier stage of the ice-covered period being the strongest during the first few weeks after ice formation.

In the absence of buoyancy production from external sources, ice-covered lakes approach a quasi-steady thermally stratified state, with water temperatures increasing nearly linearly downward from the freezing point at the ice-water boundary to values close to the maximum density of fresh water at the bottom of the lake ([7, 8]). The situation can dominate for a large part of the year in numerous Arctic lakes with long-lasting snow cover and without significant inflows. However, such lakes cannot a priori be assumed to be motion-free. With surface temperatures fixed at the freezing point, lakes remain inevitably stably stratified with regard to density, which stratification can produce water flow at the bottom of the lake by interaction with irregular bathymetry. A particular mechanism of a density-driven flow in stratified fluids without external forcing was first described by Phillips [9] and Wunsch [10] in application to deep oceanic currents: if the sidewalls are not aligned with the gravity vector, the combined effect of buoyancy force and diffusion produces bending of otherwise horizontal isopycnals at the bottom slopes in the normal to bottom direction. It results in a higher rate of accumulation of the diffusing component near the wall than within the fluid itself and propels an upward gravity flow along the slope [11, 12].

The no-flux condition at the solid boundary is essential for development of the flow. It requires the isopycnal (isothermal) surfaces to be locally perpendicular to the slope, $\frac{\partial \rho}{\partial \eta} = 0$ (where η is the wall-normal coordinate (Fig. 1)). As a result, the fluid adjacent to the sloping boundary has a different density compared to the fluid at the same elevation away from the boundary. This density difference creates a buoyancy force that drives the flow up the underlying slope. The kinetic energy of this motion is derived from the internal energy of the fluid through diffusion [9, 10, 13].

1.1 General characteristics of the diffusion-driven boundary flow

The remarkable feature of flow generation in the absence of any external forcing led to a number of laboratory, theoretical, and numerical studies on the characteristics of this flow pattern [13–17]. Peacock et al. [14] experiments focused on the dependence of the velocity in the buoyancy layer on the inclination angle ([14]). Woods [15] also examined the impact of the boundary flows on mixing within enclosed basins. Page et al. [16, 17] derived a compatibility condition that relates the mass flux and the temperature gradient along the edge to determine the re-circulation and temperature perturbations in the larger-scale "outer flow" region.

According to theoretical estimates [9, 10, 14], the velocity along the inclined wall u as a function of the normal coordinate η (Fig. 1), is defined as

$$u(\eta) = 2\kappa\gamma\cot\alpha e^{-\gamma\eta}\sin(\gamma\eta) = u_0 e^{-\gamma\eta}\sin(\gamma\eta) \tag{1}$$

where

$$\gamma^{-1} = \left(\frac{N^2\sin^2\alpha}{4\nu\kappa}\right)^{-1/4} \tag{2}$$

is the characteristic buoyancy layer thickness, κ is the molecular diffusion coefficient, ν is the kinematic viscosity, α is the wall inclination angle, $N = (-g/\rho_0\frac{\partial\rho}{\partial z})^{1/2}$ is the buoyancy frequency, g is the acceleration of gravity, ρ is the fluid density, ρ_0 is the reference density, and z is the vertical coordinate (positive upwards).

The total flux associated with the boundary flow $Q = \int_0^\infty u(\eta)d\eta = \kappa\cot\alpha$ is a function of diffusivity and slope and is independent of stratification [14]. The average velocity associated with the flow $\bar{u} = Q\gamma = \kappa\gamma\cot\alpha$ is approximately half the maximum velocity $u_{max} = \sqrt{2}e^{-\pi/4}\kappa\gamma\cot\alpha$, which occurs at $\gamma\eta = \pi/4$. The typical scales of the flow for thermal stratification ($\kappa \sim 10^{-7}$ m^2 s^{-1}, $\nu \sim 10^{-6}$ m^2 s^{-1}) are $\bar{u} \sim 10^{-3}$ m s^{-1} and $\gamma^{-1} \sim 10^{-4}$ m, respectively [13].

1.2 Potential effects on lake-wide circulation

Despite the apparently low current speeds, diffusion-driven circulation may significantly affect dynamics of ice-covered lakes being the only mechanism of deep water renewal in the absence of energy supply from the bottom or from the solar radiation under ice. This quasi-insulated state may last for several months in the majority of high-latitude lakes during the polar night. Thus, this kind of circulation may be a key regulator of biochemical processes at the water-sediment interface by supplying oxygen-saturated waters from the upper parts of the lake, and, on the other hand, may transport heat and nutrients to the upper layers, potentially affecting the ice growth rates and stimulating primary production under ice.

In an enclosed lake, the upward boundary currents should be balanced by a downward flow in the lake interior, creating a cell-like circulation. When other sources of buoyancy production are negligible, this flow is essential for maintaining circulation in ice-covered lakes and may become the primary process responsible for renewing the deep waters and supplying heat to the ice base. The low velocity magnitudes suggest that circulation due to diffusion flow in lakes is generally affected by earth rotation as

long as the currents remain slow with regard to the characteristic horizontal scale of the lake L and the Coriolis acceleration f, as expressed by the Rossby number [2, 18],

$$R_0 = \bar{u}/fL \tag{3}$$

According to previous studies [19, 20], the formation of two vertically superimposed lake-wide vertical circulation cells with downslope currents in the upper part of the lake and upslope ones beneath is accompanied by the development of two counter-rotating lake-wide gyres driven by the Coriolis effect. Rahm [19] was, to our knowledge, the first to propose a conceptual model of lake-wide circulation driven by diffusion boundary flow. He projected the model results on the lake circulation observed by Likens and Ragotzkie [21] and suggested that non-insulated sloping boundaries would strongly affect the circulation pattern by the heat release from the sediment. Following another study by Likens and Ragotzkie [22], the low vertical velocities ($\sim 10^{-6}$ m s^{-1}) suggest a strong contribution of the Coriolis force to this type of lake circulation, further complicating the circulation pattern as a function of lake dimensions.

In shallow lakes, the diffusion boundary flow may coexist with circulation driven by release of residual heat from lake sediment producing gravity currents along the bottom slope from shallow littoral towards the deeper areas of the lake [6, 23]. Converging in the deep interior of the lake, the flow can produce an upwelling in the center of the lake [2, 24]. Consequently, the resulting circulation may involve two opposing mechanisms, creating concurrent up- and downslope boundary currents at different depths [19, 21].

The diffusion boundary flow eliminates the normal to bottom density gradients at the inclined boundary that may suggest a dome-shaped bending of temperature isolines (isotherms) across the entire a lake (Fig. 2a) eventually producing a density-driven residual circulation in the water body outside of the boundary regions. Existing observations in ice-covered lakes in mid-winter are rare and do not reveal clear dome-shaped isotherm distributions. In small lakes, bending of isotherms can be observed near the bottom slopes (Fig. 2b) but not in the lake interior. In larger lakes, with characteristic length scales of several kilometers, the shape of isotherms is strongly affected by the internal basin-scale waves, which have typical time scales from hours to days [1] and mask quasi-stationary small-scale density flows (Fig. 2c). Thus, estimating the contribution of the diffusion-driven flow to lake-wide circulation from observational data is complicated.

Numerical circulation modeling represents an alternative approach, which allows to reveal qualitative and, to a certain degree, quantitative characteristics of the diffusion-driven circulation as a function of lake dimensions, shape, stratification strength, and earth rotation.

This study investigates the diffusion-density-driven circulation within a thermally stratified lake by using a three-dimensional circulation model on idealized lake bathymetry. The primary objectives of the study are:

- identifying three-dimensional circulation patterns resulting from diffusion-gravity flows along lateral boundaries in enclosed stratified lakes without external forcing.
- quantifying the effects of the lake basin dimensions, bottom slope angle, and earth rotation on the boundary flow and the residual lake-wide circulation.
- discussing the potential role of the diffusion-driven circulation in transport of heat and mass in real ice-covered lakes.

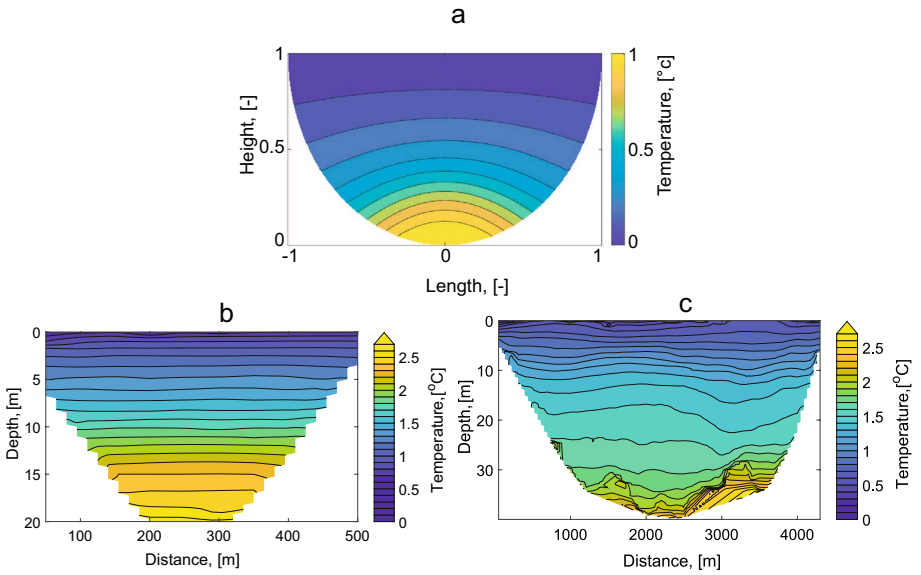

Fig. 2 **a** Hypothetical shape of isotherms in an enclosed stratified lake with insulated boundaries. **b**, **c** Cross-lake temperature transects taken in polar lakes (**b**) Saanajärvi and (**c**) Kilpisijärvi, Finland in mid-winter. The two lakes are set about 2.5 km apart at approximately 69.05°N and 20.80°E and were sampled at two subsequent days of January 2017. Temperatures were obtained from CTD casts with vertical resolution of 3×10^{-2}m (0.3 m s^{-1} lowering speed. 10Hz sampling rate) using Rinko-Profiler (JFE Advantech, Japan), temperature sensor accuracy 0.01 K

While the effect of flow generation by a sloping boundary in a density-stratified fluid has been investigated under laboratory conditions, our understanding of its role in natural environmental flows remains limited. Apart from the deep ocean, ice-covered lakes are the primary natural environments where this phenomenon can significantly influence circulation on a lake-wide scale. Understanding the interactions between diffusion-driven flow, residual circulation, and Earth's rotational effects is crucial for accurately modeling circulation patterns in ice-covered lakes and predicting their responses to changing environmental conditions [1]. Our study aims to advance knowledge by elucidating the qualitative role of diffusion-driven flow in lake-wide circulation and its interplay with other major circulation drivers beneath lake ice.

2 Methods

2.1 Model configuration and parameterizations

The simulations were run on a modified version of the Regional Ocean Modeling System (ROMS 3.9) [25, 26]. ROMS is a three-dimensional primitive equation model for flow, mass and heat transport using the terrain following vertical σ-coordinate system and the Arakawa-C horizontal grid for solving the Reynolds-averaged Navier–Stokes equations using hydrostatic and Boussinesq approximations.

Using terrain following σ-coordinates is a widely used approach to modeling stratified lakes with varying bottom topography and stratification. The terrain-following coordinates allow a higher resolution in the bottom boundary layers following the lake topography. However, σ-coordinate models are sensitive to the joint effect of steep bathymetry and vertical density stratification, resulting in pressure gradient errors. The slopes can be particularly steep near the lake shores, and the internal pressure gradient errors associated with the σ-coordinate can be significant even at high spatial resolution. ROMS implements specific algorithms to minimize these errors ([27–29]). Also, recent advances in high-performance computing make it possible to reduce the numerical errors by increasing the model resolution ([30]). Several studies [31–33] emphasized the importance of carefully selecting both horizontal and vertical grid size and resolution to ensure hydrostatic consistency. The pressure gradient error associated with σ-coordinates decreases quadratically with both vertical and horizontal grid sizes [33]. To ensure accurate simulations, sensitivity tests were conducted to determine optimal grid sizes and resolutions in the σ-coordinate system. As quantitative estimates of the internal pressure gradient errors we used the maximum grid stiffness ratios expressed as the Beckmann-Haidvogel Number (rx0) and the Haney Number (rx1) [27]. rx1 ≤ 3 is considered "safe" and conservative and IPG errors are minimal in this range [25]. For Beckmann-Haidvogel Number, $0 \leq$ rx0 ≤ 0.4 is used as a general guideline for controlling IPG errors. In our model setup the Haney Number rx1 varied between 2.89 and 4, while the Beckmann-Haidvogel Number rx0 was between 0.23 and 0.33, indicating that the grid resolution is well within the range where pressure gradient errors are expected to be minimal and ensuring the robustness of the simulations.

Instead of considering a real lake of complex bathymetry, we adopted a simulation domain of an idealized axisymmetric shape to capture the flow characteristics dependence on the lake-wide integral characteristics, such as the lake horizontal size, the maximum depth, and the mean bottom slope angle (Fig. 3a). The lake bathymetry was approximated by a Gaussian shape, describing the lake depth H as a 2-dimensional function of horizontal coordinates x_R and y_R,

$$H = H_0 e^{-S^2 \frac{(x_R^2 + y_R^2)}{R^2}} \tag{4}$$

where H_0 is the maximum lake depth at the coordinates origin $x_R = y_R = 0$, $L = 2R$ is the lake length at the surface, and S is the "shape factor" determining the steepness of the bottom slope.

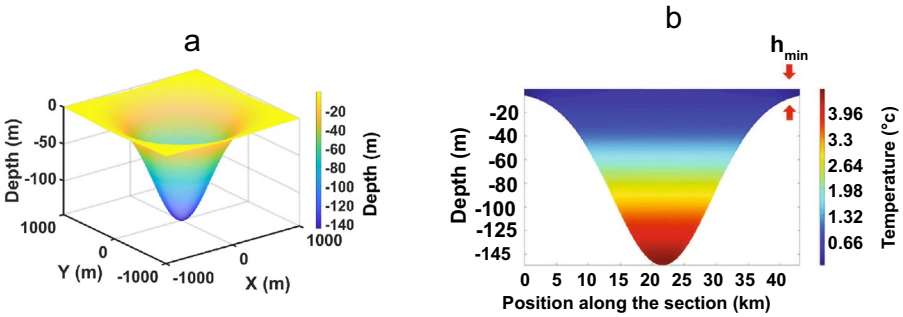

Fig. 3 Initial modeling assumptions: **a** conical bathymetry (axisymmetrical), **b** initial temperature distribution (cf. Fig. 2)

The domain dimensions were chosen based on typical depths of lakes in the range 15-150 m. The horizontal size was set based on the relative importance of the Coriolis acceleration for the lake-wide circulation characterized by the ratio of the horizontal scale of the flow (lake size) L to the Rossby radius

$$L_R = C/f, \tag{5}$$

where C is the phase speed (celerity) of the first-mode long gravity wave in a basin of depth H ($H << L$). Table 1 summarizes the domain dimensions and the corresponding first mode baroclinic Rossby deformation radii L_R. The horizontal model grid had 500×500 cells corresponding to the horizontal grid resolution from 0.8 m to 90 m, depending on the lake size. In order to ensure the stability of the numerical solution, the time step varied between 0.01 and 50 s keeping the Courant-Friedrichs-Lewy (CFL) criterion ≤ 0.85. The applicable range $\sin(\alpha)$ for each depth in the model is summarized in the third column of Table 1.

In addition to standard terrain-following transformations, the vertical spacing of the σ -grid was adjusted to the variable depth of the lake, with a higher vertical resolution near the surface and near the bottom by nonlinear stretching of the vertical coordinate depending the on local water depth [29, 34]. For the vertical resolution, two alternative setups with 30 (for shallow lakes) and 100 σ-levels (for deep lakes) were used to obtain vertical resolution ≤ 1 m in the surface and bottom boundary layers. To avoid errors produced by the convergence of multiple sigma layers in shallow areas, we set a minimum depth h_{min} at the lateral boundaries to 3 % of the maximum lake depth (H_0) (Fig. 3b). The value of h_{min} was determined from sensitivity model runs: if the value was too small, the model had a maximum density error and blew up after the 3-10 time steps (the maximum speed and the density anomaly exceeded the thresholds of 20 m s^{-1} of 200 kg m^{-3}, respectively).

The surface temperature was fixed at the freezing point of freshwater 0 °C simulating the conditions at the ice base. Vertical stratification was initiated by the linear downward temperature increase across the water column from 0 °C at the surface to the freshwater maximum density temperature at the deepest point (Fig. 3b) simulating typical thermal conditions in mid-winter lakes isolated from external heat sources ([1]). Initial temperature field was homogeneous in the horizontal plane.

Instead of applying a rigid lid boundary condition, we set up the isothermal conditions with zero momentum flux at the surface.

For simulation of the bottom friction, several sensitivity runs were performed using linear, logarithmic, and quadratic bottom stress parameterizations. The bottom friction parameterization had no remarkable effect on the modeling results, and the linear bottom friction of the momentum was eventually applied. For the lateral boundaries (i.e vertical walls at $z < h_{min}$) we tried both no-slip and free-slip conditions, which did not affect the modeling results because these shallow regions were dominated by the bottom mixing. Finally, series

Table 1 Summary of numerical domain dimensions used in model experiments. Depth H_0, the corresponding baroclinic Rossby radius L_R, buoyancy frequency N, the dimensionless lake diameter L/L_R, and the range of bottom slope angles for each depth

H_0 (m)	N (s^{-1})	L_R (m)	L/L_R					$sin(\alpha) \approx 2H_0/L$
150	$2.0{\cdot}10^{-3}$	4800	0.1	0.94	4	6	10	0.0062-0.59
75	$2.9{\cdot}10^{-3}$	2400	0.1	1.04	4	6	10	0.0062-0.59
50	$3.5{\cdot}10^{-3}$	1600	0.3	0.94	4	6	10	0.0062-0.20
25	$5.0{\cdot}10^{-3}$	800	0.3	1.6	4	6	10	0.0062-0.20
15	$6.5{\cdot}10^{-3}$	500	0.2	0.9	4	6	10	0.0062-0.30

of model experiments were performed with additional buoyancy production by the heat release from lake sediment. Constant bottom heat fluxes in the range between 0.5 W m^{-2} and 5 W m^{-2} were applied along the lake bottom corresponding to typical values reported previously by observational studies in small ice-covered lakes [6, 21, 24].

In the absence of detailed observational data on diffusion-driven flows in ice-covered lakes, the model outcomes were compared with the theoretical estimates of the current velocity $u(\eta)$ (Eq. 1) and the boundary layer thickness γ^{-1} (Eq. 2). The modeled values of the boundary layer thickness were estimated as $\gamma^{-1} = (\pi/4)^{-1}\eta_{max}$, where η_{max} is the height above the bottom of the maximum along-bottom velocity $du/d\eta = 0$ (cf. Eq. 1 and Fig. 1), and the coordinate η is equivalent to the terrain-following coordinate σ.

The effect of the bottom slope angle was investigated in terms of the aspect ratio $\beta = 2H_0L^{-1}$ and the mean slope value $\sin\alpha \approx \tan\alpha = \beta$, where H_0 and L are lake depth and lake length, respectively. The angle of the bottom slope can also be adjusted by changing the shape factor S in Eq. (4): At $S \approx 1.67$, the mean slope is approximately equal to the aspect ratio $\beta = H_0/R$. For $S > 2$, the maximum slope is about twice β, for $S > 3$, the maximum slope is about 3β. Several sensitivity tests were performed for the angle of the bottom slope by both changing $\sin\alpha$ and S for constant H_0.

The effect of the earth rotation on the circulation pattern was investigated by varying the Coriolis parameter f within the range $0{-}1.45 \times 10^{-4}$ s^{-1}, the latter value corresponding to the geographical latitude of 85°. f did not vary spatially because of the small lake dimensions compared with the planetary scales. Rotational characteristics of the lake-wide circulation were analyzed in polar coordinates (r, θ) with the origin in the lake center, and the radial velocity component and the tangential velocity components $u_r = u\cos(\theta) + v\sin(\theta)$ and $u_\theta = -u\sin(\theta) + v\cos(\theta)$, respectively.

ROMS includes several advanced schemes for calculating vertical mixing, including 2-equation turbulence models [35, 36] and k-profile parameterization [37]. However, the absence of external momentum input in the modeled circulation suggests very low mixing rates and no local production of turbulence. Therefore, we abandoned complex turbulence schemes in favor of a simple approximation of constant values of viscosity ν and temperature conductivity κ. The constrains of the circulation model related to its spatial and temporal resolution do not allow direct resolution of molecular heat and momentum fluxes. Besides, the existing observational studies on mixing conditions in ice-covered lakes [6, 7, 38] suggest an increased level of background mixing characteristic of intermittent turbulence resulting from breaking large-amplitude internal waves on the background of weak thermal stratification [1, 39]. To ensure numerical stability and to take into account background mixing production unresolved by the model algorithms, we adopted in our simulations $\nu = \kappa = 10^{-5}$ m^2 s^{-1}. While these values exceed the molecular exchange rates in the laminar boundary layer, they allow to perform simulations of lake-wide flows in a wide range of lake dimensions and to trace thereby the qualitative effects of the diffusion-driven flow on the residual circulation. These values agree with the average lake-wide mixing rates of $0.1\text{-}0.5 \cdot 10^{-4}$ m^2 s^{-1} obtained from tracer observations [38], temperature records [6, 7], and boundary-layer turbulence measurements [2, 5]. Therefore, we suggest that the artificial mixing introduced in the model can partly reflect the enhancement of the boundary flow by the background turbulence.

Horizontal and vertical advection schemes for temperature and passive tracers were calculated by the recursive flux-corrected MPDATA algorithm with a flux limiter [40]. The nonlinear equation of state was adopted, as formulated by [41, 42], assuming zero salinity. The model was run until the circulation arrived at a steady state (daily horizontal and vertical velocity profiles reached equilibrium, as well as the volume averaged kinetic energy

oscillates quasi-periodically around an equilibrium value), which took about 24-30 model days.

3 Results

3.1 Characteristics of the modeled boundary layer flow

Starting from the initial no-motion state, it took about 24 days (large lakes) to 30 days (small and shallow lakes) of model time to achieve a quasi-equilibrium state, defined by the rate of change of the mean kinetic energy within the domain dropping below 1% of its initial value. An upward boundary flow developed along the bottom slopes with the velocities of $\mathcal{O}(10^{-3})$ m s^{-1}. The numerical solution compared well with the analytical estimates of the flow rate and the boundary layer thickness demonstrating plausible model results on flow direction and structure despite the model constraints of the Boussineq and hydrostatic approximations and the necessarily coarse resolution with regard to the viscous and diffusion scales. The current velocity of the upward boundary flow varied between 0.1×10^{-3}m s^{-1} and 4×10^{-3}m s^{-1}. Variations of the shape factor S in Eq. (4) did not significantly affect the vertical velocity structure and magnitude, indicating that the boundary flow was governed by the lake-wide mean bottom slope (aspect ratio $\tan\alpha = 2HL^{-1}$) rather than local spatial gradients. Several scenarios with different aspect ratios were conducted with mean slope varying in the range from 0.35° to 40°. Both the modeled boundary layer thickness γ^{-1} and maximum velocity of the boundary flow U_{max} closely followed the theoretical dependence on the bottom slope α (Fig. 4) and agreed quantitatively with theoretical estimates following from Eqs. (1 and 2) assuming $\nu = \kappa = 10^{-5}\, m^2$ s^{-1}. Here we stress that these values exceed the molecular values and produce correspondingly higher γ^{-1} and U_{max} than those in a purely laminar boundary flow. However, the theoretical solution (Eqs. 1-2) retains its qualitative features at different ν and κ and can thereby serve as a benchmark for interpretation of the modeled flow behavior at various bottom slopes. According to the theoretical solution, the boundary flow velocities and the corresponding thickness of the bottom boundary layer decrease to zero with the slope angle α approaching 90° ($\cot\alpha \to 0$). For the steepest slope $\sin(\alpha) \approx 0.6$ ($H_0 = 150$ m, $L/2 = 240$ m, see Table 1), the modeled maximum velocities were $< 5 \times 10^{-4}$m s^{-1}, and the boundary layer thickness was ~ 0.1m,

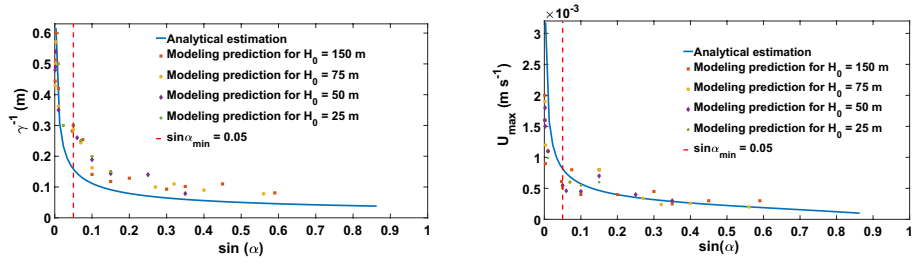

(a) γ^{-1} (m) ($\nu = \kappa = 10^{-5}$) (b) U_{max} (m s^{-1}) ($\nu = \kappa = 10^{-5}$)

Fig. 4 Comparison of modeling results (points) against analytical estimation (blue lines) for **a** the boundary layer thickness γ^{-1} and **b** maximum upward current velocity U_{max} at different values of the bottom slope $\sin\alpha$. Note: Modeled results at different depths are depicted using distinct point colors

close to those predicted by the scaling (Eq. 1). At very small α, the solution (Eqs. 1-2) becomes invalid, producing infinite growth of flow velocities at $\alpha \to 0$. Wunsch [10] proposed a lower threshold of the bottom slope, where the theory is still valid, to scale as

$$\sin \alpha_{min} = C_R R^{-1/4}, \tag{6}$$

based on the Rayleigh number

$$R = \frac{N^2 \Lambda^4}{\nu \kappa}, \tag{7}$$

where Λ is the "characteristic length scale of stratification" and C_R is a proportionality coefficient. The modeled velocities deviated from the theoretical formula to lower values at $\sin \alpha \lesssim 0.05$ (Fig. 4b). Adopting the lake depth for the characteristic length scale $\Lambda \approx H_0$, the typical values of the Rayleigh number in our numerical experiments amounted at $R \approx 7 \times 10^{-4}$, and the critical slope $\sin \alpha_{min} = 0.05$ corresponds to $C_R \approx 70$ in Eq. (6). At this point, a direct comparison with the laboratory experiments of Peacock et al. [14] is insightful for further interpretation of our modeling results: in their laboratory setup, the dimensions were about two orders of magnitude smaller than in our modeling domain, compensated by much stronger salinity-driven stratification $N \approx 2\ \mathrm{s}^{-1}$, which resulted in a similar value of the Rayleigh number $R \approx 8 \times 10^{-4}$. The experiments of Peacock et al. [14] yielded $\sin \alpha_{min} \approx 0.05$, which agrees with our model outcomes. Two important intermediate conclusions can be made based on this agreement: (i) our model simulations captured the same regime of the diffusion-driven flow modeled previously in the lab, suggesting their applicability at wider range of spatial scales, (ii) the Rayleigh-based scaling is valid for the critical slope estimates, and the proportionality coefficient can be suggested to be $10^1 \le C_R \le 10^2$.

3.2 Residual flow and lake-wide circulation in a non-rotating domain

The model simulated an upward current along sloping boundaries and a downwelling return flow over the bulk of the lake's water column Fig. 5a, b. In the horizontal plane, the flow converged toward the lake center in the upper layers and diverged in the lower layers (Fig. 6a, c). Around the mid-depth, the downward residual flow got balanced by the divergence due to upward currents along the slopes. As a result, a converging frontal zone in a

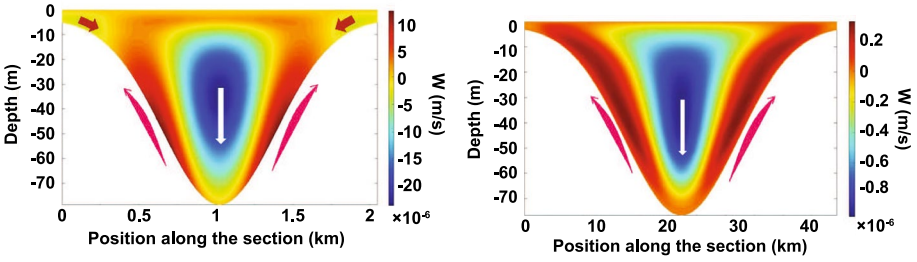

Fig. 5 Cross-section of vertical velocity magnitudes in a 75 m deep domain for a lake width of **a** 2 km and **b** 40 km. Positive velocity direction is upward

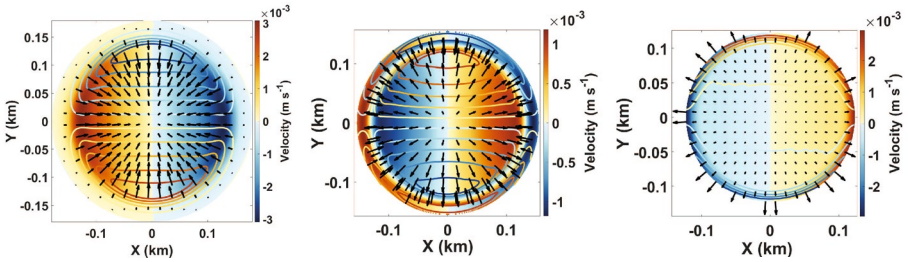

(a) 5 m (b) 15 m (c) 50 m

Fig. 6 Horizontal velocity transect in a non-rotating lake at water depth **a** 5 m, **b** 15 m, and **c** 50 m. Color is the x velocity component, isolines show the y velocity component, arrows show current vectors in relative units

Table 2 L_{min} for different lake depths

Depth (m)	150	75	50	25	15
L_{min} (km)	16	8	6	4	3
β	0.10	0.10	0.12	0.16	0.20

horizontal plane was created there, with an outward flow in the center of the lake and an inward flow near the shores (Fig. 6b).

The intensity of circulation increased with growing domain size: Maximum vertical velocities in the smallest modeled domain ($L = 240$ m and $H_0 = 75$ m) reached 0.2×10^{-6}m s^{-1} and 0.01×10^{-6}m s^{-1} for downward and upward flow, respectively. For the largest domain ($L = 45$ km and $H_0 = 150$ m), the respective values were 8.0×10^{-6}m s^{-1} and 6.0×10^{-6}m s^{-1}. The smaller magnitudes of the upward flow are caused by the larger part of the lake volume being occupied by the upflow and by concentration of the upward flow within the narrow boundary layer at the bottom slopes (cf. Figs. 4 and 5).

In domains with a large bottom slope, apart from the downward residual flow in the central part of the lake, converging downward currents existed in shallow areas (Fig. 5a), driven apparently by slowing down of the upward boundary currents near the surface. The shallow downward flow disappeared if the aspect ratio $\beta = HL^{-1}$ decreased below ~ 0.15. The effect might be artificially produced by the specific Gaussian-like bottom profile but can still be relevant for natural lakes with a large shallow littoral area surrounding a deeper lake interior. The threshold values of the horizontal dimensions L_{min} (the smallest length scale at which modeling outcomes did not exhibit downward flow in shallow areas) are summarized in Table 2 for different lake depths.

3.3 Effect of heat flow from sediment

The general effect of the added heat source at the lake bottom Q_B consisted in cancelling of the upward diffusion-driven boundary flow replaced by downward boundary currents due to negative buoyancy production at the slopes and an upward return flow in the lake interior. This single-cell pattern dominated the vertical circulation in all simulations for shallow lakes ($H_0 \leq 25$ m) within the entire range of typical bottom heat flux values $Q_B = 0.5 - 5.0$ W m^{-2},

as well as in deeper lakes of $H_0 \gtrsim 25$ m with relatively small lateral dimensions $L \lesssim 20$ km and a strong bottom heat flux $Q_B \gtrsim 1.5\text{W m}^{-2}$ (Fig. 7a).

In the vertical plane, downward boundary currents converged towards the deepest part of the lake resulting in a return upward flow in the interior of the lake diverging near the surface (Fig. 7a).

Variations of the shape factor S in Eq. (4) did not significantly affect the structure and magnitude of the vertical velocity. The intensity of circulation increased with growing domain size: Within the bottom heat flux range 0.5-3.0 W m^{-2}, the maximum current velocities of the downward boundary flow varied between $0.2\text{-}0.4 \times 10^{-4}$m s^{-1} in small ($L = 0.48$ km) lakes and $2.5\text{-}4.0 \times 10^{-4}$m s^{-1} in large ($L = 45$ km) lakes. Maximum horizontal velocities varied between 3×10^{-3}m s^{-1} at horizontal domain scale $L = 45$ km and 7×10^{-3}m s^{-1} at $L = 0.48$ km. The upward residual flow had typical magnitudes of 2×10^{-6}m s^{-1}.

At low bottom flux magnitudes $Q_B \lesssim 1.5\text{W m}^{-2}$ and large lake dimensions $L \gtrsim 20$ km, the vertical flow pattern was more complex, revealing a "double boundary layer" with features of both diffusion-driven currents and gravity currents due to heat flux at the bottom: An upward movement persisted along the boundaries compensated by a downward jet-like return flow immediately above (Fig. 7b). Apparently, the flow pattern reflects the situation when the two opposed buoyancy gradients along the bottom slope created by the diffusion-viscosity effects and by the heat release from the sediment are nearly equal in their magnitude. Both flows arise from buoyancy effects at the solid boundary, with velocities increasing away from the bottom in a direction perpendicular to the slope. If the diffusion boundary layer is thinner than the gravity boundary layer created by heat flux from the sediment, the diffusion-driven flow reaches its peak closer to the bottom, and the superposition of the two boundary layers would result in the downward flow is positioned above the upward flow, which explains the modeled "double boundary layer" structure (Fig. 7b). The mean upslope velocity of the diffusion flow $\bar{u}$ is given by Eq. (1). In turn, the mean downward velocity due to bottom heat flux can be scaled following Terzhevik et al. (2009) as (see Eq. 9 in [6])

$$u_* \propto \left(q_B \cot\alpha\right)^{1/2} \left(agH_0\right)^{-1/4},$$

where q_B [K ms^{-1}] is the kinematic (divided by the water density and heat capacity, $\rho C_p \approx 4.2 \times 10^6$) [J K^{-1} m^{-3}]) heat flux from the sediment, and a [K^{-2} is the coefficient in the quadratic equation of state accounting for its non-linearity in the vicinity of T_{md}. Equating $\bar{u} = u_*$ results in the scaling relationship

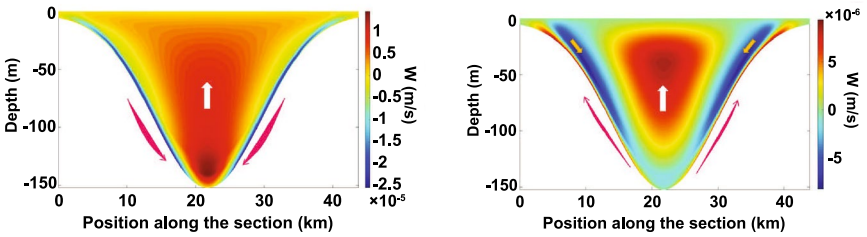

(a) $Q_B = 3\ \text{W m}^{-2}$ (b) $Q_B = 0.5\ \text{W m}^{-2}$

Fig. 7 Vertical velocity in a lake with dimensions $L = 40$ km, $H_0 = 150$ m at (a) strong bottom heat flux, $Q_B = 3$ W m^{-2} and (b) weak bottom heat flux, $Q_B = 0.5$ W m^{-2}. Upward velocities are positive

$$Nu^{1/2}Pr^{1/4} = \sqrt{\cos\alpha/2}, \tag{8}$$

where $Nu = \frac{q_B H_0}{\kappa \Delta T}$ is the Nusselt number and $Pr = \frac{\nu}{\kappa}$ is the Prandtl number. In our model configuration, $\cos\alpha \approx 1$, which reduces the condition of the "double boundary layer" development to $Nu = 1/2$. The upward diffusion boundary flow should prevail at $Nu \ll 1/2$, and the downslope flow driven by q_B dominates at $Nu \gg 1/2$. The threshold values of the domain dimensions L_{min} and H_0, and the bottom heat flux Q_{max} at which "double boundary layer" developed are summarized in Table 3. The Nusselt number varied in the range 0.25–1.50. While close to the theoretical threshold of 0.5, the critical Nu slightly increased with increasing lake depth H_0. The fact can be tentatively ascribed to the role played by nonlinear advective effects at increasing lake dimensions but is not taken into account in the quasi one-dimensional scaling (Eq. 8).

In the vertical plane, a divergent flow from the center of the lake towards lake shoreline close to the surface was surrounded by a narrow convergence belt along the boundaries as a result of upward boundary currents. Additionally, a residual upward current existed in the central region of the lake. The maximum current velocity of boundary flow in this case was as high as 2×10^{-3}m s^{-1} ($L = 45$ km and $H_0 = 50$ m) and 4×10^{-3}m s^{-1} ($L = 45$ km and $H_0 = 150$ m) for $Q_B = 0.5$ W m^{-2}.

3.4 Re-adjustment of thermal stratification

For diffusion-driven flow with no heat flow across the bottom, the modeled temperature distributions showed bent isotherms within the narrow buoyant boundary layer (Fig. 8a) in accordance with the theory predicting redistribution of density to eliminate the normal-to-bottom component of the density gradient (Fig. 1) and similar to observations in shallow ice-covered lakes (Fig. 2b). Outside the relatively thin boundary layer of thickness $\sim \gamma^{-1}$, vertical stratification remained however undisturbed, with strictly horizontal isotherms across the lake interior, being in contrast to the tentative assumption of smooth dome-like shaping of isotherms across the entire lake in an asymptotic steady state (Fig. 2a).

Model runs with a strong bottom heat flux ($Q_B > Q_{max}$ or $Q_B < Q_{max}$ and $L < L_{min}$) produced upward bending of isotherms near the bottom slopes extending deep into the lake interior (Fig. 8c). The intermediate situation with (Q_B) $< Q_{max}$ and $L \geq L_{min}$ exhibited a downward change of isotherms curvature sign from concave shape near the surface to bottom-flux dominated convex shape in the lower part of the water column (Fig. 8b).

3.5 Rotation effects on the circulation

With the Coriolis force included into the model equations, at domain sizes exceeding the Rossby radius $L \gg L_R$, an anticyclonic circulation developed in the upper part of the lake (Fig. 9a), with the flow converging towards the center. In the lower part of the water column,

Table 3 Threshold values Q_{max} and L_{min} for development of a "double boundary layer" at different lake depths

H_0 (m)	150	75	50
Q_{max} (W m^{-2})	2	1.5	1.25
L_{min} (km)	18	19	22
Nu	1.50	0.67	0.25

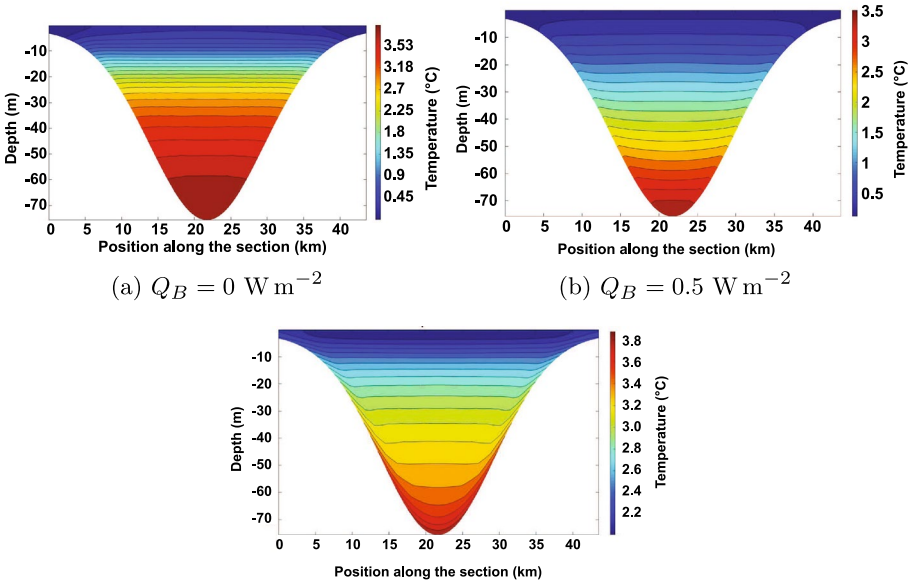

(a) $Q_B = 0$ W m^{-2} (b) $Q_B = 0.5$ W m^{-2}

(c) $Q_B = 3$ W m^{-2}

Fig. 8 Modeled temperature distributions in a 75-m deep lake **a** without bottom heat flux, **b** with a weak bottom heat flux, and **c** with a strong bottom heat flux

the circulation reversed to cyclonic (Fig. 9c), with corresponding divergence towards the perimeter. The change in lake rotation took place at water depth between 5 to 25 m, depending on the lake's size and depth, as illustrated by the profile of the horizontally averaged azimutal component of current velocity in polar coordinates $\overline{u_\theta}$ (thick solid line in Fig. 9b). For a constant maximum lake depth H_0, the rotation strength decreased with decreasing horizontal dimensions L (thick solid line and line with square symbol in Fig. 9b). Vertical distribution of the radial velocity component (dotted line in Fig. 9b) reflects the two-cell circulation pattern, demonstrating a converging flow in the upper anticyclonic gyre and divergence in the cyclonic gyre underneath.

A comparison of the flow characteristics in large lakes to those in lakes with $L \leq L_R$ (lines with symbols in Fig. 9b) reveals the major qualitative effects of the Coriolis force on the three-dimensional flow pattern: For both $L \gg L_R$ and $L \leq L_R$, the radial flow demonstrates the same vertical structure with convergence in the upper water column and divergence in the deeper layers (Fig. 9b, $\overline{u_r}$ blue line with diamond markers for $L \leq L_R$, and orange dashed line for $L \gg L_R$). However, in large, rotation-affected lakes the magnitudes of the radial currents are lower, and part of the kinetic energy is transferred to the azimutal flow. The latter is in turn nearly absent in small lakes except the boundary layer, where a weak anticyclonic rotation is generated by the combined effect of narrowing topography and downward velocity decrease due to the bottom shear. The Coriolis effect also reduces the thickness of the upper anticyclonic layer in large lakes compared by about 20% to small ones.

Another remarkable effect of the Coriolis force consisted in cancelling the near-shore shallow downward flow, which existed in large lakes without rotation (cf. Fig. 5): the downslope currents weakened with increased horizontal dimensions and eventually ceased at $L/L_R \gtrsim 3$ for $H_0 > 50$ m and $L/L_R \gtrsim 4$ for $H_0 < 50$ m).

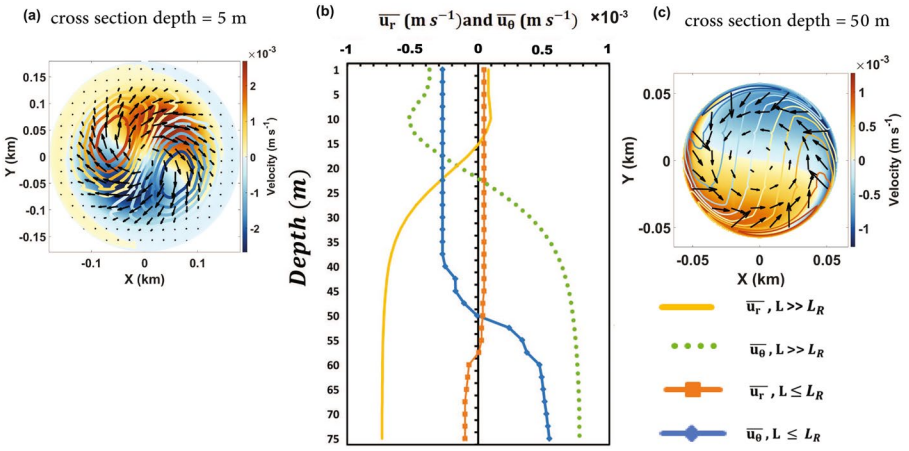

Fig. 9 Horizontal velocity transect in a rotating lake with H_0 =75 m and $Q_B = 0$ W m^{-2} at water depth **a** 5 m and **c** 50 m. Color is the x velocity component, isolines show the y velocity component, arrows show current vectors in relative units. **b** vertical profiles of horizontally averaged velocity components in polar coordinates. Solid orange line and dotted green line are the azimuthal $\overline{u_\theta}$ and radial $\overline{u_r}$ components at $L > L_R$, respectively. Lines with markers are $\overline{u_\theta}$ (squares) and $\overline{u_r}$ (diamonds) for $L \le L_R$. Positive u_r corresponds to outward flow; positive u_θ corresponds to clockwise rotation

Incorporating of a bottom heat flux into the rotating model domain creates a two-gyre system with a cyclonic gyre occupying the upper part of the lake and anticyclonic rotation in deeper layers (Fig. 10a–c) in agreement with the change of the boundary flow from upward to downward. This rotation pattern retains for $Q_B > Q_{max}$ as well as $Q_B < Q_{max}$ and $L < L_{min}$ (Table 3). In turn, in a large domain with relatively low bottom heat flux ($Q_B < Q_{max}$ and $L > L_{min}$) the flow additionally separates in the horizontal plane into an anticyclonic circulation in the central region of the lake and a cyclonic circulation near the shoreline (Fig. 11a).

The vertical distribution of the radial and azimuthal velocity components demonstrates a pattern reverse to that without rotation (Fig. 10): a cyclonic rotation in the upper part of the water column changes to an anticyclonic gyre at depths below 5-20 m. Similar to the model results without a bottom heat flux, rotation reduces the vertical position of the boundary between divergent and convergent flows: if the upper 2/3 of the non-rotating water column was occupied by a divergent flow (Fig. 10b blue line with diamond markers), the Coriolis force reduces the thickness of this layer to $< 1/3H_0$ (Fig. 10b green dotted line).

4 Discussion

The phenomenon of an inclined solid boundary generating momentum in an initially quiescent stratified fluid has drawn the attention of fluid mechanics experts and oceanographers over the past half-century [9, 10, 13]. Alone the self-propulsion of neutrally buoyant solid bodies, such as a horizontal wedge submerged in a stably stratified medium, inspired several theoretical and laboratory studies and a discussion on the possible significance of this effect in natural fluids [13, 43, 44]. While the majority of previous studies were focused on characteristics of the thin boundary layer adjacent to the solid boundary, our research centered on the potential effect of the diffusion-driven flow on the basin-scale circulation in ice-covered lakes, where the

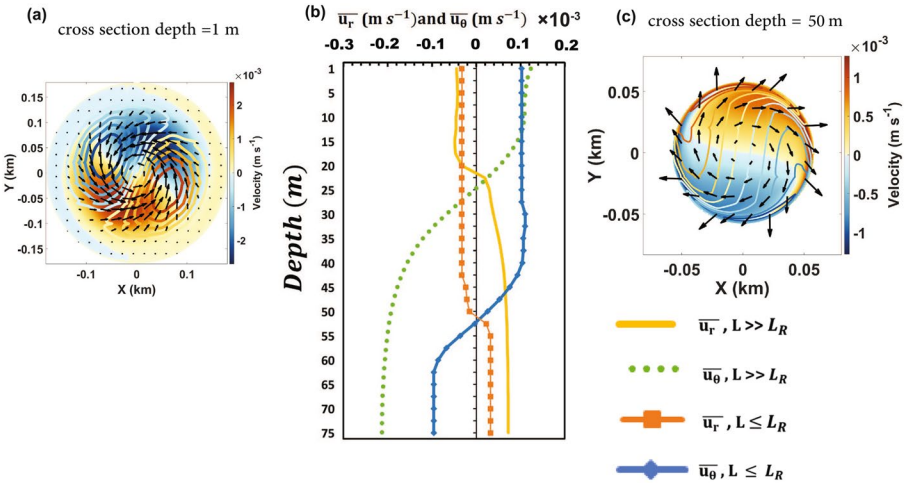

Fig. 10 Same as Fig. 9 but for $Q_B = 3$ W m^{-2}

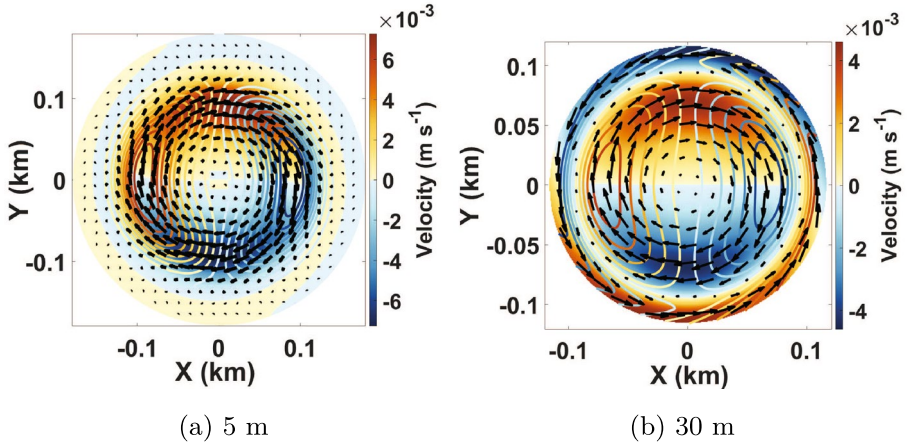

Fig. 11 Horizontal velocity transects at lake depths 5 m and 30 m in a 40 m wide lake with $Q_B = 0.5$ W m^{-2}. Color is the x velocity component, isolines show the y velocity component, arrows show current vectors in relative units. The scale of velocity vectors has been adjusted for greater readability

boundary flow induce a circulation pattern that plays a crucial role in the renewal of deep water and the vertical transport of solutes across the water column.

Simulations with the ROMS model demonstrated the ability of a hydrostatic Boussinesq σ -coordinate model to emulate initiation of the upward boundary flow along the bottom slopes. The qualitative agreement of the model outputs with the expected diffusion-driven flow pattern was further investigated by applying scenarios with different aspect ratios and variations of the mean bottom slope α in the range between 0.35° and 40°. The modeled boundary layer thicknesses and current velocities at different bottom slopes agreed well with the theoretical estimates (Eqs. 1- 2) supporting the adequate simulation of the boundary flow by the model.

The modeling results not only closely followed the theoretical predictions but also indicated cancelling of the flow at $\sin\alpha < 10^{-1}$. The result allows to put a lower threshold of the validity of the theoretical solution (Eqs. 1-2), which produces infinite growth of flow velocities at $\alpha \to 0$. Originally, Wunsch [10] proposed a lower threshold of the bottom slope, where the theory is still valid to depend on the Rayleigh number of the flow (Eq. 6). Our results confirm the Rayleigh number scaling with a proportionality coefficient of ~ 70, which is close to the scaling derived from laboratory experiments by Allshouse et al. and Peacock et al. [13, 14] at much smaller flow dimensions and stronger density stratification. We conclude therefore that Eq. (6) with the depth of the flow as a characteristic length scale and the coefficient of $\mathcal{O}(10^1)$ is a reliable estimate of the minimum slope required for initiation of the viscous boundary flow.

Despite the good qualitative agreement of the model outcomes with the theory and the previous laboratory experiments, the modeled flow magnitudes should be interpreted with care. The terrain-following models are effective for simulating the bottom boundary layer, but errors in internal pressure gradient estimation can lead to artificial flow [27]. While these errors typically converge to zero with the square of the grid size [31, 33], they can still cause significant artificial flow in coarse resolution studies where topography and stratification are less well resolved [45]. Furthermore, selecting both horizontal and vertical grid sizes and resolutions is important to ensure hydrostatic consistency [31]. The numerical viscosity and diffusion inherent to discrete circulation modeling do not allow direct simulation at scales corresponding to the molecular values $\kappa \sim 10^{-7}$ m^2 s^{-1} and $\nu \sim 10^{-6}$ m^2 s^{-1}. We were able to obtain stable model configuration with constant viscosity and diffusion coefficients in the range 10^{-5}-10^{-4} m^2 s^{-1}, where a stronger diffusion had to be set up for larger lake dimensions (coarser numerical grid resolution). Apparently, the increased mixing rates affect the estimates of the flow magnitude and the boundary layer thickness compared with the purely diffusion-driven flow observed in the lab [13, 14]. On the other hand, studies on ice-covered lakes [1, 6, 38] report background diffusion values of $1.0\text{-}5.0 \times 10^{-5}$ m^2 s^{-1}, which are close to those implemented in the model, and the natural circulation pattern can deviate from the laboratory simulations towards the modeling results, i.e. the numerically-conditioned high mixing in the model can to some degree imitate the natural enhancement of boundary layer mixing.

4.1 Lake-wide circulation

In an enclosed lake, the upward boundary flow at the bottom slopes initiates a cell-like circulation with a downward return flow in the bulk of the lake. The downward flow rates depend on the ratio of the boundary layer thickness to the horizontal scales of the lake and are accordingly low for typical lake dimensions: The downward flow rates depend on the ratio of the boundary layer thickness to the horizontal scales of the lake and are accordingly low for typical lake dimensions: the along-bottom upward boundary current of $\mathcal{O}(10^{-3})$ s^{-1} produces lake-wide circulation with vertical flow components of $\mathcal{O}(10^{-6})$ s^{-1}. The rates are however high enough to produce a full overturn in a 2.5 m deep lake within a month, whereas a 15 m deep lake would have been mixed to the bottom within 6 months. Taking into account the long duration of the ice-covered period in polar lakes, the majority of shallow post-glacial and thermokarst lakes in these regions are prone to be significantly affected by this type of circulation in the absence of solar heating and a weak heat flow across the sediment. In addition to the one-cell lake-wide overturn in the vertical plane, the model sometimes predicted convergence flow in shallow nearshore areas. The effect might be artificially produced by the specific Gaussian-like bottom profile, but can be relevant for natural lakes with large shallow littoral areas surrounding a deeper lake interior.

4.2 Effect of heat flow from sediment

The added heat source at the lake bottom (Q_B) counteracts the diffusion-driven upward boundary flow and replaces it with downward boundary currents and an upward return flow in the lake interior. This single-cell circulation pattern dominates in all simulations except large lakes ($L \gtrsim 20$ km) with low bottom heat flux magnitudes ($Q_B \lesssim 1.5$ W m^{-2}), where the boundary layer features both diffusion-driven upward currents and downward gravity currents due to the heat flux at the bottom. Hence, the diffusion-gravity flow can dominate lake circulation in lakes with very low heat release from the sediment, e.g. thermokarst lakes in permafrost areas, or deep and large lakes, which accumulate low amount of heat during the ice-free period. The modeled range of downslope gravity currents, $0.2\text{-}4.0 \times 10^{-4}$m s^{-1}, is supported by available estimates from ice-covered lakes: Welch et al. [24] reported sinking velocities of $\mathcal{O}(10^{-4})$ s^{-1} in the bottom boundary layer of a lake with sediment heat release of about 3 W m^{-2}. The same field study reported upward return flow of $\mathcal{O}(10^{-6})$ s^{-1}, which is also in agreement with our model estimates. On the other hand, the scaling analysis performed by Terzhevik et al. [6] on temperature records from boreal Lake Vendyurskoe (Russia) yielded the downslope current velocities as high as 2×10^{-3} m s^{-1} for the bottom heat flux of 5 W m^{-2}. These outcomes of an order-of-magnitude scaling analysis can be interpreted as the uppermost velocity estimates, taking into account the rather high value of the bottom heat flux. Therefore, we conclude that our model results are generally close to what can be found in real lakes, at least for the gravity currents driven by the heat release from the sediment in relatively small lakes.

4.3 Effects of rotation

According to our results, the Coriolis force strongly affects the three-dimensional flow patterns in the majority of ice-covered lakes: at characteristic velocities $\bar{u} = \mathcal{O}(10^{-3})$ m s^{-1} and corresponding high latitudes, $f = \mathcal{O}(10^{-4})$, the Rossby number (3) becomes essentially small at lake dimensions $> 10^2$ m. The Coriolis effect on the flow patterns in large lakes ($L \gg L_R$) consists in partial transformation of radial velocities into azimuthal (tangential) ones. On lake-wide scales, it produces a lake-wide anticyclonic gyre in the upper water column dominated by convergent flow and a cyclonic gyre in the deep divergent part (Fig. 9a). Thereby, Coriolis force weakens radial currents in large lakes and reduces the thickness of the upper convergent layer. The strength of rotation reduces with decreasing lake length scale, and at $L \leq L_R$, only the weak anticyclonic rotation retains in the deepest part of the lake.

Incorporating a bottom heat flux changes the direction of the circulation with a cyclonic gyre in the upper part of the lake and an anticyclonic gyre in the deeper layers. A more complex rotational pattern develops in the "intermediate" situation, where both diffusion-driven mechanism and heat release from the sediment contribute to the circulation. In the latter case, the flow separates into an anticyclonic circulation in the lake's central region and an cyclonic circulation near the shoreline (Fig. 11c, d). Similar to the circulation pattern without bottom heat flux, rotation weakens the radial flow and reduces the thickness of the upper divergent layer from the upper two-thirds of the water column in non-rotating conditions to less than one-third of the total depth.

Our results elaborate on the previous conceptual [19] and numerical [20] models of lake circulation under ice driven by the sediment heat release. Rahm [19] used a bulk one-dimensional model for the circulation in an idealized lake with constant heat input from sediments of $0.6 - 0.9$ W m^{-2} to obtain a two-cell circulation in the vertical plane with downward currents along the bottom slope and a compensating upward flow in the upper part of the water column.

The simple model suggested this circulation cell to cease at around half of the entire lake depth, while the lower part of the lake was dominated by the diffusion-driven circulation.

Our results suggest more complex circulation pattern, where both downward and upward boundary flows always persist across the entire lake depth, and may co-exist at weak heat release from the sediment, creating a “double boundary layer” with an upward movement along the solid boundaries and a downward jet-like return flow immediately above. While the qualitative mechanisms producing the “double boundary layer” are plausible, and the modeled conditions of its formation agree well with the zero-dimensional scaling of major buoyancy-producing forces, it should be noted that modeling results assume a smooth bottom as well as simplified turbulence and bottom boundary mixing parameterizations. In natural lakes, factors such as bottom roughness and shear mixing between opposing flows may lead to be more complex flow patterns than a clear two-layer structure. Nevertheless, the modeling outcomes offer a preliminary estimate of lake dimensions and flux magnitudes, capturing an "intermediate" scenario where both driving mechanisms are important for lake circulation. In this regard, observations by Likens and Ragotzkie [21] in Tub Lake can me mentioned, who revealed a two-cell structure in 1961, and a simple one-cell circulation pattern in the previous year. The observations indicate that the circulation pattern can vary between years, depending on the amount of heat stored in the sediment and the stratification in the lake water column.

A two-cell circulation was also obtained in numerical simulations by Huttula [20], who applied a three-dimensional model to examine circulation in ice-covered lakes in a configuration with constant temperature boundary conditions at the lake bottom slopes. Consequently, the value of the bottom heat flux varied with depth. Similar to our results, the upper cell in their model occupied the uppermost 20 m of the 87-m deep water column. However, the reported velocities of $> 1 \times 10^{-3}$m s^{-1} were an order of magnitude higher than in our study that can be tentatively ascribed to a much coarser spatial resolution of the model. In summary, we suggest that, despite the constrains of the numerical modeling, our results are quantitatively closer to what can be expected in natural lakes.

Detailed fine-scale measurements are necessary to validate and complement the modeling results and provide a better insight into the role of the gravity flows in under-ice circulation. In turn, the outputs of the model can serve as a benchmark for measurements and a background for design of field experiments. Existing mid-winter observations are scarce, and the small current speeds make it challenging to estimate the contribution of diffusion-driven flow to lake-wide circulation.

5 Conclusions

We tested the ability of primitive equation hydrostatic models to simulate the diffusion-driven flow driven at an inclined solid boundary in a stratified fluid and investigated the potential effects of the diffusion-driven flow on the basin-scale circulation in ice-covered lakes, which remain stably stratified and virtually free from external buoyancy production for extended periods. The model reproduced qualitative, and, with some degree of uncertainty, quantitative features of the flow, aligning well with theoretical predictions, and allowed establishing the minimum bottom slope required for the boundary flow to exist as a function of stratification and vertical length scale. The study revealed several characteristics of circulation in enclosed lakes: In the absence of buoyancy production at the bottom, the residual circulation overturns the entire lake water column within 1 to 6 months, and may significantly contribute to heat and mass transport in many shallow lakes with long ice-covered seasons. When additional buoyancy is produced by

the heat flux from lake sediment, a counterflow emerges, resulting in a complex circulation pattern characterized by the superposition of two opposing boundary flows. At flux magnitudes as high as several W m^{-2}, the counterflow can completely replace the diffusion-driven circulation. Due to the small magnitudes of these flows, the Coriolis effect substantially influences the circulation in most lakes, except the smallest ones, and partially transforms radial flow into rotational lake-wide "gyres". The number and rotational direction of these gyres depend on the relative contribution of the bottom heat flux. While the uncertainty in the quantitative estimates is inevitable due to the artificially increased mixing and potential effects of the pressure gradient errors, the modeling outcomes provide a framework for designing field studies in real lakes and investigation of circulation effects on transport of nutrients, dissolved oxygen, and greenhouse gases in ice-covered lakes.

Acknowledgements The study is part of the project IceTMP (Project ID 01LP2006A) funded by The Federal Ministry of Education and Research (BMBF) within the framework of the Strategy "Research for Sustainability" (FONA). Georgiy Kirillin was supported by the German Research foundation (Project DFG KI 853/16-1 "LaMer"). Additional support by the DFG PRoject "PycnoTrap" GR 1540/37-1 is thankfully acknowledged by GK. T.H. acknowledges funding through the Research Council of Norway through its Centres of Excellence funding scheme via iC3: Centre for ice, Cryosphere, Carbon and Climate (project number 332635). The authors gratefully acknowledge the computing time granted by the Resource Allocation Board and provided on the supercomputer Lise and Emmy at NHR@ZIB and NHR@Göttingen as part of the NHR infrastructure. The calculations for this research were conducted with computing resources. We thank Thomas Mehner and the participants of the workshop 'Scientific Writing' at the Leibniz Institute of Freshwater Ecology and Inland Fisheries (IGB Berlin) for helpful discussion on the early stage of the manuscript.

Author contributions GK and FS conceived the study; FS performed model adjustment and modeling experiments; FS and GK performed the core analysis of results and drafted the ms; FS, RH, TH and GK contributed to final analysis and writing.

Funding Open Access funding enabled and organized by Projekt DEAL.

Declarations

Conflict of interest This study is performed within the framework of the Strategy "Research for Sustainability" (FONA) of The Federal Ministry of Education and Research (BMBF). The authors have no relevant financial or non-financial interests to disclose.

References

1. Kirillin G, Leppäranta M, Terzhevik A, Granin N, Bernhardt J, Engelhardt C, Efremova T, Golosov S, Palshin N, Sherstyankin P et al (2012) Physics of seasonally ice-covered lakes: a review. Aquat Sci 74(4):659–682
2. Kirillin G, Forrest A, Graves K, Fischer A, Engelhardt C, Laval B (2015) Axisymmetric circulation driven by marginal heating in ice-covered lakes. Geophys Res Lett 42(8):2893–2900
3. Mironov D, Terzhevik A, Kirillin G, Jonas T, Malm J, Farmer D (2002) Radiatively driven convection in ice-covered lakes: observations, scaling, and a mixed layer model. J Geophys Res Oceans 107(C4):7
4. Winters KB, Ulloa HN, Wüest A, Bouffard D (2019) Energetics of radiatively heated ice-covered lakes. Geophys Res Lett 46(15):8913–8925

5. Rizk W, Kirillin G, Leppäranta M (2014) Basin-scale circulation and heat fluxes in ice-covered lakes. Limnol Oceanogr 59(2):445–464
6. Terzhevik A, Golosov S, Palshin N, Mitrokhov A, Zdorovennov R, Zdorovennova G, Kirillin G, Shipunova E, Zverev I (2009) Some features of the thermal and dissolved oxygen structure in boreal, shallow ice-covered Lake Vendyurskoe, Russia. Aquat Ecol 43(3):617–627
7. Malm J, Terzhevik A, Bengtsson L, Boyarinov P, Glinsky A, Palshin N, Petrov M (1997) Temperature and salt content regimes in three shallow ice-covered lakes: 2 heat and mass fluxes. Hydrol Res 28(2):129–152
8. Dibike Y, Prowse T, Saloranta T, Ahmed R (2011) Response of northern hemisphere lake-ice cover and lake-water thermal structure patterns to a changing climate. Hydrol Process 25(19):2942–2953
9. Phillips O (1970) On flows induced by diffusion in a stably stratified fluid. Deep-Sea Res Oceanogr Abstr 17(3):435–443
10. Wunsch C (1970) On oceanic boundary mixing. Deep-Sea Res Oceanogr Abstr 17(2):293–301
11. Ivey G, Corcos G (1982) Boundary mixing in a stratified fluid. J Fluid Mech 121:1–26
12. Phillips O, Shyu J-H, Salmun H (1986) An experiment on boundary mixing: mean circulation and transport rates. J Fluid Mech 173:473–499
13. Allshouse MR, Barad MF, Peacock T (2010) Propulsion generated by diffusion-driven flow. Nat Phys 6(7):516–519
14. Peacock T, Stocker R, Aristoff JM (2004) An experimental investigation of the angular dependence of diffusion-driven flow. Phys Fluids 16(9):3503–3505
15. Woods AW (1991) Boundary-driven mixing. J Fluid Mech 226:625–654
16. Page MA, Johnson ER (2008) On steady linear diffusion-driven flow. J Fluid Mech 606:433–443
17. Page MA, Johnson ER (2009) Steady nonlinear diffusion-driven flow. J Fluid Mech 629:299–309
18. Ramón CL, Ulloa HN, Doda T, Winters KB, Bouffard D (2021) Bathymetry and latitude modify lake warming under ice. Hydrol Earth Syst Sci 25(4):1813–1825
19. Rahm L (1985) The thermally forced circulation in a small, ice-covered lake. Limnol Oceanogr 30(5):1122–1128
20. Huttula T, Pulkkanen M, Arkhipov B, Leppäranta M, Solbakov V, Shirasawa K, Salonen K (2010) Modelling circulation in an ice-covered lake. Estonian J Earth Sci 59(4):298
21. Likens GE, Ragotzkie RA (1965) Vertical water motions in a small ice-covered lake. J Geophys Res 70(10):2333–2344
22. Likens GE, Ragotzkie RA (1966) Rotary circulation of water in an ice-covered lake: with 6 figures and 1 table in the text. Int Vereinigung Theor Angewandte Limnol Verhandlungen 16(1):126–133
23. Mortimer C, Mackereth F (1958) Convection and its consequences in ice-covered lakes: with 5 figures and 2 tables in the text and on 1 folder. Int Vereinigung Theor Angewandte Limnol Verhandlungen 13(2):923–932
24. Welch HE, Bergmann MA (1985) Water circulation in small arctic lakes in winter. Can J Fish Aquat Sci 42(3):506–520
25. Ocean Modeling Group, DMCS: regional ocean modeling system (ROMS). https://www.myroms.org/
26. Shchepetkin AF, McWilliams JC (2009) Ocean forecasting in terrain-following coordinates: formulation and skill assessment of the regional ocean modeling system. J Comp Phys 227:3595–3624
27. Shchepetkin AF, McWilliams JC (2003) A method for computing horizontal pressure-gradient force in an oceanic model with a nonaligned vertical coordinate. Journal of Geophysical Research: Oceans, 108(C3)
28. Haidvogel DB, Beckmann A (1999) Numerical ocean circulation modeling. World Scientific, London
29. Song Y, Haidvogel D (1994) A semi-implicit ocean circulation model using a generalized topography-following coordinate system. J Comput Phys 115(1):228–244
30. Berntsen J, Thiem O, Avlesen H (2015) Internal pressure gradient errors in σ-coordinate ocean models in high resolution fjord studies. Ocean Model 92:42–55
31. Haney RL (1991) On the pressure gradient force over steep topography in sigma coordinate ocean models. J Phys Oceanogr 2:610
32. Beckmann A, Haidvogel DB (1993) Numerical simulation of flow around a tall isolated seamount. Part I: problem formulation and model accuracy. J Phys Oceanogr 23(8):1736–1753
33. Mellor GL, Oey L-Y, Ezer T (1998) Sigma coordinate pressure gradient errors and the seamount problem. J Atmos Oceanic Tech 15(5):1122–1131
34. Haidvogel DB, Arango HG, Hedstrom K, Beckmann A, Malanotte-Rizzoli P, Shchepetkin AF (2000) Model evaluation experiments in the north atlantic basin: simulations in nonlinear terrain-following coordinates. Dyn Atmos Oceans 32(3–4):239–281
35. Mellor GL, Yamada T (1982) Development of a turbulence closure model for geophysical fluid problems. Rev Geophys 20(4):851–875
36. Umlauf L, Burchard H (2005) Second-order turbulence closure models for geophysical boundary layers. A review of recent work. Cont Shelf Res 25(7–8):795–827

37. Large WG, McWilliams JC, Doney SC (1994) Oceanic vertical mixing: a review and a model with a nonlocal boundary layer parameterization. Rev Geophys 32(4):363–403
38. Colman JA, Armstrong DE (1983) Horizontal diffusivity in a small, ice-covered lake. Limnol Oceanogr 28(5):1020–1026
39. Kirillin G, Engelhardt C, Golosov S, Hintze T (2009) Basin-scale internal waves in the bottom boundary layer of ice-covered lake Müggelsee, Germany. Aquat Ecol 43(3):641–651
40. Smolarkiewicz PK, Margolin LG (1998) Mpdata: a finite-difference solver for geophysical flows. J Comput Phys 140(2):459–480
41. Jackett DR, Mcdougall TJ (1995) Minimal adjustment of hydrographic profiles to achieve static stability. J Atmos Ocean Tech 12(2):381–389
42. Millero FJ, Poisson A (1981) International one-atmosphere equation of state of seawater. Deep sea research part A. Oceanogr Res Papers 28(6):625–629
43. Page MA (2010) Propelled by diffusion. Nat Phys 6(7):486–487
44. Mercier MJ, Ardekani AM, Allshouse MR, Doyle B, Peacock T (2014) Self-propulsion of immersed objects via natural convection. Phys Rev Lett 112(20):204501
45. Berntsen J, Furnes G (2005) Internal pressure errors in sigma-coordinate ocean models-sensitivity of the growth of the flow to the time stepping method and possible non-hydrostatic effects. Cont Shelf Res 25(7–8):829–848

Authors and Affiliations

Fatemeh Sadat Sharifi[1,2] · Reinhard Hinkelmann[2] · Tore Hattermann[3] · Georgiy Kirillin[1]

✉ Fatemeh Sadat Sharifi
fatemeh.sharifi@igb-berlin.de

Reinhard Hinkelmann
reinhard.hinkelmann@wahyd.tu-berlin.de

Tore Hattermann
Tore.Hattermann@npolar.no

Georgiy Kirillin
georgiy.kirillin@igb-berlin.de

[1] Department of Ecohydrology and Biogeochemistry, Leibniz Institute of Freshwater Ecology and Inland Fisheries, Müggelseedamm 310, 12587 Berlin, Germany

[2] Department of Planning Building Environment, Faculty VI-Planning Building Environment, Institute of Civil Engineering, Chair of Water Resources Management and Modeling of Hydrosystems, Technische Universität Berlin, Gustav-Meyer-Allee 25, 13355 Berlin, Germany

[3] Department of Physics and Technology, UiT The Arctic University of Norway, Sykehusvegen 23, 9019 Tromsø, Norway